

# Mechanistic Strategies in the HDV Ribozyme: Chelated and Diffuse Metal Ion Interactions and Active Site Protonation

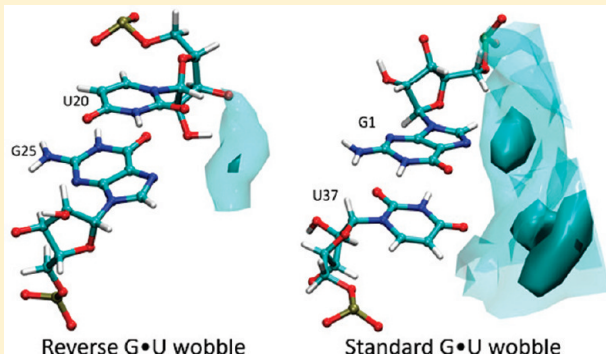
Narayanan Veeraraghavan,<sup>†</sup> Abir Ganguly,<sup>‡</sup> Barbara L. Golden,<sup>§</sup> Philip C. Bevilacqua,<sup>\*,†,‡</sup> and Sharon Hammes-Schiffer<sup>\*,‡</sup>

<sup>†</sup>Huck Institutes of Life Sciences and <sup>‡</sup>Department of Chemistry, 104 Chemistry Building, The Pennsylvania State University, University Park, Pennsylvania 16802, United States

<sup>§</sup>Department of Biochemistry, Purdue University, 175 South University Street, West Lafayette, Indiana 47907, United States

**S** Supporting Information

**ABSTRACT:** The crystal structure of the precleaved form of the hepatitis delta virus (HDV) ribozyme reveals two G•U wobbles near the active site: a rare reverse G•U wobble involving a *syn* G base, and a standard G•U wobble at the cleavage site. The catalytic mechanism for this ribozyme has been proposed to involve a Mg<sup>2+</sup> ion bound to the reverse G•U wobble, as well as a protonated C75 base. We carried out molecular dynamics simulations to analyze metal ion interaction with the reverse and standard G•U wobbles and to investigate the impact of C75 protonation on the structure and motions of the ribozyme. We identified two types of Mg<sup>2+</sup> ions associated with the ribozyme, chelated and diffuse, at the reverse and standard G•U wobbles, respectively, which appear to contribute to catalysis and stability, respectively. These two metal ion sites exhibit relatively independent behavior. Protonation of C75 was observed to locally organize the active site in a manner that facilitates the catalytic mechanism, in which C75<sup>+</sup> acts as a general acid and Mg<sup>2+</sup> as a Lewis acid. The simulations also indicated that the overall structure and thermal motions of the ribozyme are not significantly influenced by the catalytic Mg<sup>2+</sup> interaction or C75 protonation. This analysis suggests that the reaction pathway of the ribozyme is dominated by small local motions at the active site rather than large-scale global conformational changes. These results are consistent with a wealth of experimental data.



## I. INTRODUCTION

RNA enzymes, or ribozymes, can use both metal ions and nucleobases in their catalytic mechanisms. Large ribozymes tend to rely on the positioning of divalent ions to stabilize their transition states,<sup>1,2</sup> while smaller ribozymes primarily use nucleobases to stabilize their transition states, often via proton transfer.<sup>3–5</sup> The genomic hepatitis delta virus (HDV) ribozyme, depicted in Figure 1A, is unusual in that it uses both metal ion and nucleobase catalysis in its reaction mechanism.<sup>6–8</sup> This ribozyme is comprised of five pairing regions, P1–P4 and P1.1, and the active site is found in the cleft formed between the P1/P1.1/P4 and P2/P3 coaxial stacks. Recent studies reveal that the HDV ribozyme occurs in all three kingdoms of life and is found in the human genome.<sup>9,10</sup> Study of the HDV ribozyme is thus of special interest both for how it integrates two diverse catalytic mechanisms, as well as for its importance to fundamental life processes.

We have described the mechanism of the ribozyme as multi-channel, in which three parallel channels carry out the same chemistry of phosphodiester bond cleavage using the 2'-hydroxyl of U-1 as a nucleophile.<sup>6,11</sup> All three channels appear to use C75 as the general acid to protonate the 5'-bridging oxygen of G1 but differ in their use of Mg<sup>2+</sup> ions.<sup>12–15</sup> In channel 1, Mg<sup>2+</sup> is not

present, and high concentrations of Na<sup>+</sup> promote the reaction; in channel 2, Mg<sup>2+</sup> ions serve solely structural roles, accounting for a rate acceleration of ~125-fold; and in channel 3, Mg<sup>2+</sup> serves a catalytic role, accounting for an additional ~25-fold in rate acceleration for an overall contribution of Mg<sup>2+</sup> ions to reactivity of ~3000-fold.<sup>6</sup> Figure 1B provides a schematic depiction of the mechanism in channel 3.<sup>8,16</sup> The pK<sub>a</sub> of C75 is shifted toward neutrality in all three reaction channels, enhancing its ability to serve as a general acid, although this pK<sub>a</sub> shift is opposed somewhat by Mg<sup>2+</sup> addition.<sup>13,15,17,18</sup>

The structural biology of the HDV ribozyme includes three major structures. The first was a structure of the cleaved (product) form of the ribozyme.<sup>12,19</sup> This structure revealed that C75 accepts a hydrogen bond from the leaving group 5'OH of G1, which suggested a general acid role for C75H<sup>+</sup> in the cleavage reaction according to microscopic reversibility. The second was a set of structures of the precleaved form, in which self-cleavage was inhibited by a C75U mutation or by omission of

**Received:** April 6, 2011

**Revised:** May 6, 2011

**Published:** June 07, 2011

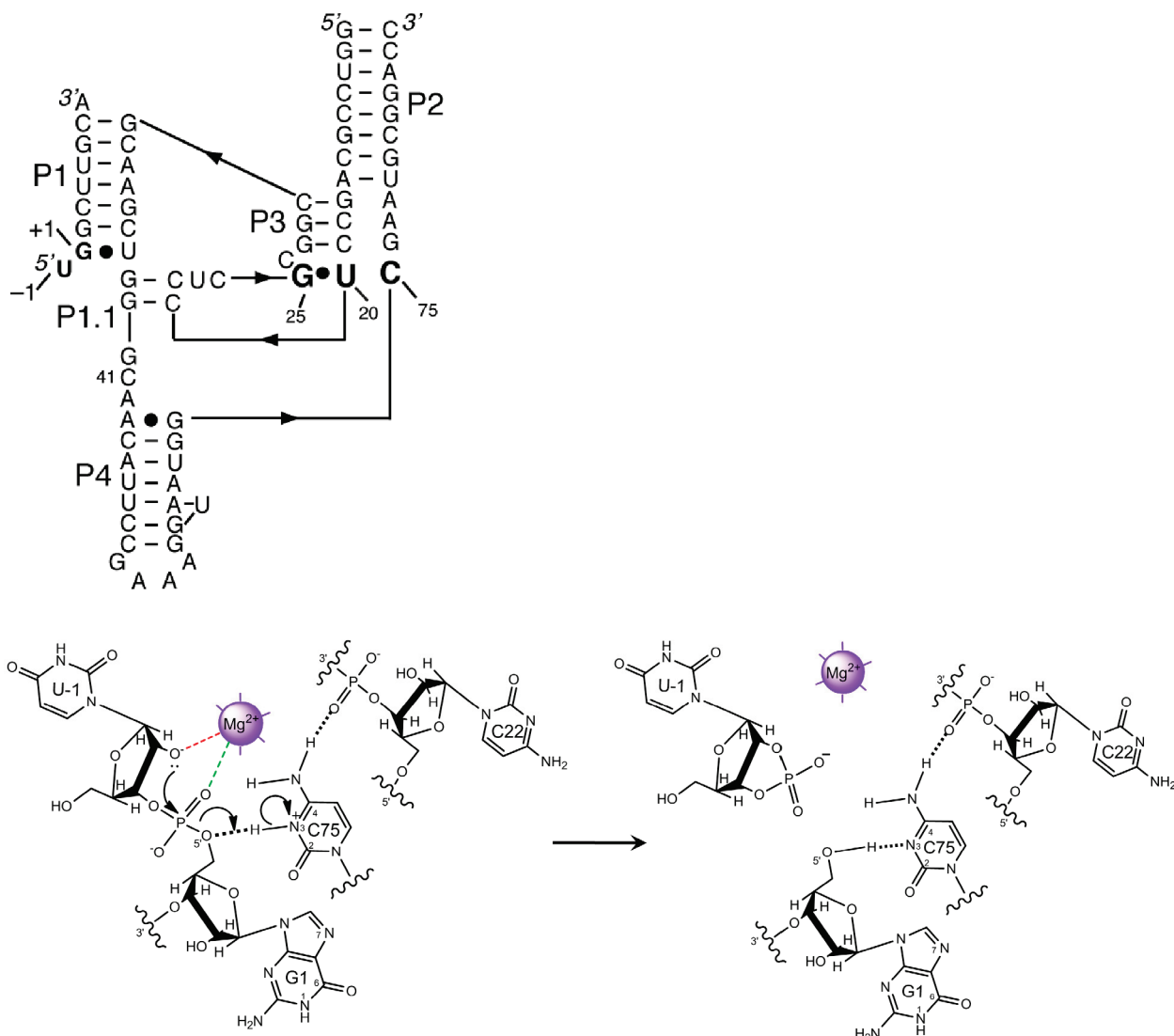


**Figure 1.** Secondary structure of the precleaved genomic HDV ribozyme and proposed mechanism. (A) Secondary structure of the precleaved HDV ribozyme (PDB ID 3NKB)<sup>8</sup> used for the MD studies. There are five pairing regions, P1–P4 and P1.1. The cleavage site is between U-1 and G1. Numbering is based on the genomic HDV ribozyme. The reverse G•U wobble and catalytic C75 residue are in large bold font. (B) Proposed mechanism of HDV ribozyme self-cleavage in which Mg<sup>2+</sup> serves as a Lewis acid and C75 serves as a general acid.<sup>8</sup>

Mg<sup>2+</sup> ions.<sup>20,21</sup> The C75U precleaved structure was similar in overall topology to the product structure, but it showed U75 in a position to serve as a general base for cleavage, with Mg<sup>2+</sup> in the general acid position. Recent evidence suggests, however, that this particular ribozyme construct is misfolded, owing to the amine-to-keto change in C to U and the inability of U to be cationic.<sup>14</sup> Recently we solved a third structure of the HDV ribozyme, which was also of the precleaved state but in the presence of Mg<sup>2+</sup> ions and with C75.<sup>8</sup> Moreover, the structure was at a low pH where C75 should remain in the protonated catalytically active state. In these crystals, the reaction was inhibited by changing the 2'-hydroxyl nucleophile of U-1 to a hydrogen.<sup>8</sup> The overall topology of the C75 precleaved structure is also similar to the product. However, unlike the C75U mutant structure, the active site of this precleaved structure was much more similar to that of the product structure, with C75 in position to serve as the general acid. Moreover, the C75 precleaved structure also revealed a Mg<sup>2+</sup> ion positioned to serve as a Lewis

acid by stabilizing a deprotonated 2'-hydroxyl of U-1. In general, the C75 precleaved structure is more consistent with a large literature of experimental biochemical studies than is the C75U structure.<sup>8,14</sup>

The HDV ribozyme active site contains both standard and reverse G•U wobbles. A standard G•U wobble (Figure 2, G1•U37) has two hydrogen bonds and is largely compatible with the A-form helix,<sup>22</sup> especially for terminal wobbles that induce less deformation of the helix.<sup>23</sup> Much less common is a reverse G•U wobble (Figure 2, G25•U20), also with two hydrogen bonds, in which the G is in the rare *syn* conformation wherein the base resides over the ribose sugar.<sup>24</sup> Notably, both of these wobbles expose functional groups that possess negative dipoles and are capable of interacting with metal ions in the major and minor grooves for standard and reverse wobbles, respectively. In the HDV ribozyme, the G and U at positions 25 and 20 are absolutely conserved,<sup>10</sup> and they interact with the putative catalytic Mg<sup>2+</sup> ion through its hydration shell.<sup>8</sup> The standard

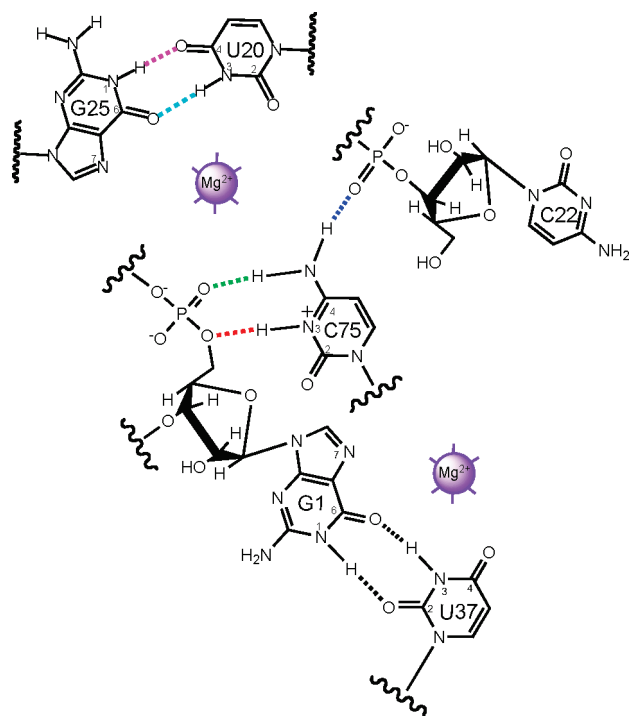


**Figure 2.** Key active site interactions in the genomic HDV ribozyme. The wobble between G25 and U20 is a reverse G•U wobble, and the wobble between G1 and U37 is a standard G•U wobble. The precleaved crystal structure shows the presence of the  $Mg^{2+}$  ion at the reverse wobble, and the  $Mg^{2+}$  ion at the standard wobble is included for illustrative purposes.

wobble between G1 and U37 is at the base of P1, where it is present in the majority ( $\sim 80\%$ ) of HDV ribozymes,<sup>25</sup> although it is sometimes replaced with Watson–Crick GC and AU base pairs in nature<sup>9,10,25</sup> with little effect on reaction kinetics or metal dependence.<sup>26</sup> Solution kinetic and Raman spectroscopic experiments suggest a structural  $Mg^{2+}$  ion may interact with the G1•U37 wobble, although this ion was not unambiguously identified in the recent crystal structure.<sup>8</sup> In addition, a G•U to AU change at the reverse wobble leads to more than a 1000-fold reduction in cleavage rate,<sup>27</sup> whereas the same change, as well as a G•U to GC change, at the standard wobble has no effect.<sup>26</sup>

We have recently combined experiments and molecular dynamics (MD) calculations on both product and precleaved HDV ribozyme structures. Studies on the product form of the ribozyme revealed long-distance communication between a structural base triple and the active site.<sup>28</sup> Subsequent studies on the C75 precleaved form of the ribozyme revealed that the rare reverse G•U wobble helps form an anionic motif in the active site that is capable of interacting with both divalent and monovalent ions.<sup>16</sup> The electrostatic potential of this site is exceptionally negative, which accommodates the experimental observations that this site can both interact strongly with divalent ions and drive protonation of C75 with a shifted  $pK_a$ , despite repulsive electrostatic interaction between the two cations. Moreover, this reverse G•U wobble was also observed in MD simulations of the product form of the ribozyme and was found to be consistent with the crystallographic data for the product form.<sup>16</sup> These studies on both the C75 precleaved and product forms of the HDV ribozyme further indicated that the reverse G•U wobble is maintained throughout the catalytic reaction.

In the present study, we investigate the impact of C75 protonation and  $Mg^{2+}$  interaction at both of the G•U wobbles on the structure as well as the motions of the HDV ribozyme. We computationally alter protonation of C75 and presence of the catalytic metal ion at the reverse G•U wobble, as well as investigate the effects of mutation of the standard G•U wobble to a Watson–Crick GC base pair. Our simulations indicate that protonation of C75 provides local organization of the active site and that the metal ion interactions are qualitatively different at the reverse and standard G•U wobbles. In addition, we find that these two metal ion sites exhibit relatively independent behavior. Finally, our calculations indicate that the overall structure and thermal motions of the ribozyme are not significantly affected by C75 protonation or metal ion interaction.

## II. METHODS

We computed MD trajectories starting with the coordinates based on the recently solved precleaved crystal structure PDB ID 3NKB.<sup>8</sup> The deoxynucleotides at positions 1 and 2 were converted to ribonucleotides by addition of 2'-hydroxyls with ideal bond lengths and bond angles. The upstream nucleotide and scissile phosphate were built as described previously,<sup>8</sup> leading to a total of 73 nucleotides in the system. Hydrogen atoms were added using Accelrys Discover Studio Visualizer 2.0. C75 was protonated at N3 for the trajectories denoted “C75<sup>+</sup>” and deprotonated for the trajectories denoted “C75<sup>-</sup>”. Residue C41 was protonated in all trajectories to allow the native base triple to form.<sup>19,28</sup> The partial charges used for protonated cytosine are provided in ref 16. The ribozyme was solvated with rigid TIP3P waters<sup>29</sup> in a periodically replicated orthorhombic box. The 10  $Mg^{2+}$  ions resolved in the crystal structure were included. The system was neutralized with  $Na^+$  ions, and physiological monovalent ionic strength was added to the solvent to give a physiological ionic strength of  $\sim 0.15$  M NaCl. The solvation of the ribozyme with pre-equilibrated water molecules and the random placement of  $Na^+$  and  $Cl^-$  ions in the bulk solvent were carried out using the Maestro utility.<sup>30</sup>

The MD calculations were performed with the Desmond MD program<sup>31,32</sup> using the AMBER99 forcefield.<sup>33,34</sup> Long-range electrostatic interactions were calculated using the Smooth Particle Mesh Ewald method<sup>35</sup> with a cutoff of 12 Å, and SHAKE constraints<sup>36</sup> were applied to bonds involving hydrogen. Following the comprehensive simulated annealing equilibration procedure described in Supporting Information, we collected 25 ns of data at 298 K in the canonical ensemble (i.e., at constant NVT) for each trajectory. A Nosé-Hoover thermostat<sup>37,38</sup> was used to maintain constant temperature, and the time step was 1 fs for all MD trajectories. For each state of the system studied, we propagated at least two independent trajectories and, in some cases, additional independent trajectories. The root-mean-square deviations of the heavy atoms with respect to the coordinates used as the starting structure for the MD trajectories are provided for the two sets of independent trajectories in Figure S13.

Electrostatic potential calculations were carried out using numerical solutions to the nonlinear Poisson–Boltzmann (NLPB) equation using the Adaptive Poisson–Boltzmann Solver (APBS), as described previously.<sup>16,39,40</sup> Structural coordinates were obtained from the starting structure used for MD. Metal ions and water molecules were omitted from the NLPB calculations, as is customary. Both C75 and C41 were protonated in the NLPB

calculations. The atomic radii and partial charges were defined using the Amber99 parameter set except for C41<sup>+</sup> and C75<sup>+</sup>, which were defined as described previously.<sup>16</sup> Three-dimensional structures were rendered using VMD,<sup>41</sup> and electrostatic potentials were rendered using PyMOL.<sup>42</sup>

We also performed additional analyses of the MD data. The root-mean-square deviations (RMSDs) and radial distribution functions (RDFs) were calculated using VMD,<sup>41</sup> and the root-mean-square fluctuations (RMSFs) of the residues, including only the heavy atoms, were calculated using GROMACS.<sup>43</sup> To examine the statistical correlation between the thermal fluctuations of pairs of atoms, we calculated the cross-correlation matrices with elements

$$S_{jk} = \frac{C_{jk}}{\sqrt{C_{jj} C_{kk}}} \quad (1)$$

The covariance matrix has elements defined as

$$C_{jk} = \langle (\mathbf{r}_j - \langle \mathbf{r}_j \rangle) \cdot (\mathbf{r}_k - \langle \mathbf{r}_k \rangle) \rangle \quad (2)$$

where the brackets denote an ensemble average over configurations. The cross-correlation matrix describes pairwise atomic motions that are either in phase (i.e., moving in the same direction) or out of phase (i.e., moving in the opposite direction).

To analyze the charge density near the G•U wobbles, we generated charge isodensity plots using VMD.<sup>41</sup> For this purpose, a cube with sides of length 12 Å was defined centered on the G25(O6) atom for the reverse G•U wobble and on the G1(O6) atom for the standard G•U wobble. The volume of this cube was divided into a grid of cubes with sides of length 1 Å. The total charge per 1 Å cube was determined by summing the charges of Mg<sup>2+</sup>, Na<sup>+</sup>, and Cl<sup>-</sup> in each 1 Å cube. The charge isodensity was plotted by filling the 1 Å grid cubes representing the greatest 30% and 80% of the charge density in the entire 12 Å cube with dark and light colors, respectively.

### III. RESULTS

The goal of our MD simulations is to determine the impact of active site nucleobase protonation and Mg<sup>2+</sup> ion interactions on the structure and motions of the HDV ribozyme, as well as to gain insight into the catalytic mechanism. Specifically, we examine the impact of C75 protonation because C75 is thought to serve as the general acid in the catalytic mechanism.<sup>6,13,14</sup> We also study the influence of the crystallographically resolved Mg<sup>2+</sup> ion at the reverse G25•U20 wobble because this Mg<sup>2+</sup> ion, denoted “Mg<sub>rev</sub>” in this paper, is also thought to be directly involved in the catalytic mechanism, acting as a Lewis acid.<sup>8</sup> To perform this analysis, we computed three types of trajectories. In the trajectories denoted “C75<sup>+</sup>/Mg<sub>rev</sub>”, C75 is protonated and the Mg<sub>rev</sub> is included in the starting structure. In the trajectories denoted “C75<sup>+</sup>/noMg<sub>rev</sub>”, C75 is protonated, but the Mg<sub>rev</sub> is removed from the starting structure prior to equilibration; in this case, two additional Na<sup>+</sup> ions are added to the bulk solvent to maintain overall charge neutrality of the system. In the trajectories denoted “C75°/Mg<sub>rev</sub>”, C75 is deprotonated, one Na<sup>+</sup> ion is added to the bulk solvent, and the Mg<sub>rev</sub> is included in the starting structure. We analyze the active site hydrogen-bonding structure in each of these trajectories. In addition, we analyze the interaction of ions with both the reverse G25•U20 wobble and the nearby standard G1•U37 wobble by generating radial distribution functions and charge isodensity plots, as well as electrostatic potentials via NLPB calculations. Finally, we analyze the atomic fluctuations

and correlated motions of the ribozyme by calculating the RMSFs and cross-correlation matrices.

**A. Active Site Hydrogen Bonding Interactions.** Three key hydrogen-bonding interactions are observed for C75 in the HDV ribozyme in the precleaved crystal structure: C75(N3) to G1-(O5'), C75(N4) to G1(O2P), and C75(N4) to C22(O2P) (Figure 2).<sup>8</sup> The time evolution of these distances is shown in Figure 3A–C for trajectories of type C75<sup>+</sup>/Mg<sub>rev</sub>, C75<sup>+</sup>/noMg<sub>rev</sub>, and C75°/Mg<sub>rev</sub> respectively. A second set of independent trajectories for each type is provided in Supporting Information (Figure S1A–C). As illustrated in Figure 3A, all three of the hydrogen bonds involving C75 are maintained throughout the first C75<sup>+</sup>/Mg<sub>rev</sub> trajectory, and similar behavior was observed for the second independent trajectory (Figure S1A). These trajectories represent the catalytically competent ribozyme because the C75 is protonated and the crystallographically resolved catalytic Mg<sup>2+</sup> is bound.

For the first C75<sup>+</sup>/noMg<sub>rev</sub> trajectory, the two hydrogen bonds between C75 and G1 are weakened for the first 10 ns but are stably formed for the remainder of the trajectory (red and green lines in Figure 3B). In the second independent trajectory (Figure S1B), these hydrogen bonds are predominantly formed for the first 5 ns but are weakened somewhat for the remainder of the trajectory, although the distances between the heavy atoms still remain less than 4 Å. The fluctuations in hydrogen bonding observed in the early portions of the trajectories indicate that the systems may not be fully equilibrated until ~5 ns or that they may exist in two or more different states involving varying degrees of hydrogen bonding. For completeness, we present all of the data from all trajectories. The conclusions of this paper are not influenced by the fluctuations observed at early times or the differences between independent trajectories of the same type. The hydrogen bond between C75(N4)-C22(O2P), which is the one not involving G1 (Figure 2, blue line), is the one hydrogen bond that is maintained throughout both trajectories. This analysis suggests that Mg<sub>rev</sub> may help stabilize the G1 phosphate group to position C75<sup>+</sup> for catalysis. This conclusion is also consistent with the inner-sphere contact between the pro-R<sub>P</sub> oxygen of G1 and Mg<sub>rev</sub> identified in the crystal structure of the C75 precleaved ribozyme.<sup>8</sup> Nevertheless, even in the absence of Mg<sub>rev</sub>, the hydrogen-bonding interactions involving C75 are maintained, although slightly weakened in some cases.

The C75°/Mg<sub>rev</sub> trajectory exhibits substantial movement of C75 away from G1 (Figure 3C). When C75 is deprotonated, there can be no direct hydrogen bonding between C75(N3) and G1(O5') as both atoms are hydrogen bond acceptors. In addition, the hydrogen bond between C75(N4) and G1(O2P) is completely absent (red and green lines in Figure 3C), and the hydrogen bond between C75(N4) and C22(O2P) is lost after ~6 ns (blue line in Figure 3C) in the first trajectory. In the second independent trajectory (Figure S1C), the hydrogen bonds between C75 and G1 are again completely absent, although the single hydrogen bond between C75(N4) and C22(O2P) is maintained throughout the trajectory. These two independent trajectories are consistent in that the hydrogen bonds between C75 and G1, which are critical for alignment for general acid catalysis, are absent; the hydrogen-bonding interaction between C75 and C22 may be intermittent. Thus, removal of the proton on N3 of C75 eliminates important hydrogen-bonding and electrostatic interactions, leading to local structural rearrangements that diminish the stability of the other two hydrogen bonds. Overlay of thermally averaged structures from

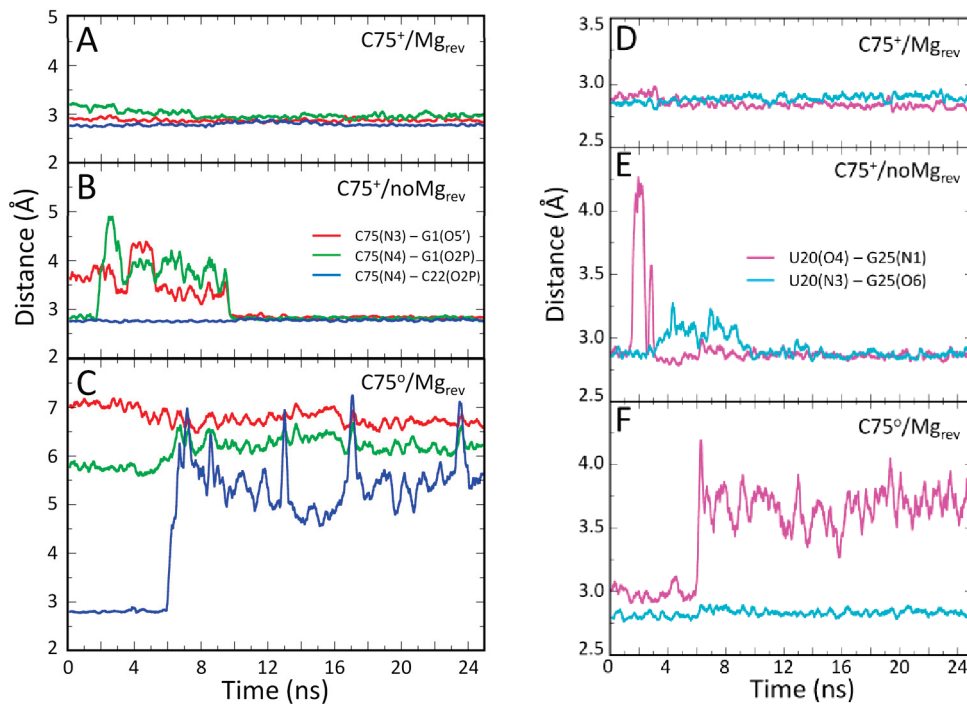


**Figure 3.** Hydrogen bonding interactions in the active site of the HDV ribozyme. The distances shown are between heavy atoms of the hydrogen-bonding interactions involving C75 (panels A–C) and within the reverse G•U wobble (panels D–F). Results are provided for the three different types of trajectories:  $\text{C75}^+/\text{Mg}_{\text{rev}}$  (panels A and D),  $\text{C75}^+/\text{noMg}_{\text{rev}}$  (panels B and E), and  $\text{C75}^\circ/\text{Mg}_{\text{rev}}$  (panels C and F). The color scheme is the same as in Figure 2.

the  $\text{C75}^+/\text{Mg}_{\text{rev}}$  and  $\text{C75}^\circ/\text{Mg}_{\text{rev}}$  trajectories (Figure S2) reveals that protonated C75 remains in a reactive alignment, whereas deprotonated C75 does not. When C75 is deprotonated, the interaction between the nucleophilic O2' of U-1 and the catalytic  $\text{Mg}^{2+}$  is also lost. The average distance between the catalytic  $\text{Mg}^{2+}$  and the nucleophilic O2' of U-1 (red hydrogen bond in Figure 1B) is  $\sim 2 \text{ \AA}$  when C75 is protonated but  $\sim 5.5 \text{ \AA}$  when C75 is deprotonated (Figure S3, red lines). For both protonation states, however, the distance between the catalytic  $\text{Mg}^{2+}$  and G1(O2P) (green hydrogen bond in Figure 1B) remains  $\sim 2 \text{ \AA}$  throughout the trajectory (Figure S3, green lines). This analysis suggests that protonation of C75 plays an important role in aligning the active site for catalysis.

Hydrogen-bonding interactions in the reverse G•U wobble were also monitored. The time evolution of these two distances is depicted in Figures 3D, E, and F for the three types of trajectories. A second set of independent trajectories for each type is provided in Supporting Information (Figure S1D–F). In the two independent  $\text{C75}^+/\text{Mg}_{\text{rev}}$  trajectories, these hydrogen bonds are stably maintained at  $\sim 2.8 \text{ \AA}$  (Figures 3D and S1D). The  $\text{Mg}_{\text{rev}}^{2+}$  ion maintains its crystallographically modeled position throughout both trajectories, interacting with U-1(O2'), G1(O2P), and U23(O1P) directly, as well as with the reverse G•U wobble via water molecules (Figure S3). The reverse G•U wobble hydrogen bonds are also maintained in the two independent  $\text{C75}^+/\text{noMg}_{\text{rev}}$  trajectories (Figures 3E and S1E), with occasional excursions in the initial part of the first trajectory. In this case, the  $\text{Mg}_{\text{rev}}$  eliminated in the starting structure is replaced by one or more  $\text{Na}^+$  ions during equilibration and throughout the trajectories, as reported previously.<sup>16</sup> This analysis indicates that the absence of  $\text{Mg}_{\text{rev}}$  does not significantly impact the hydrogen-bonding interactions within the reverse G•U wobble.

The two  $\text{C75}^\circ/\text{Mg}_{\text{rev}}$  trajectories exhibited qualitatively different behavior in this region. In the first  $\text{C75}^\circ/\text{Mg}_{\text{rev}}$  trajectory, the hydrogen bond between G25(O6) and U20(N3) is maintained throughout the trajectory, but the hydrogen bond between G25(N1) and U20(O4) is lost after  $\sim 6 \text{ ns}$ , although it increases to only  $\sim 3.7 \text{ \AA}$  (magenta line in Figure 3F). Detailed investigation reveals that deprotonation of C75 leads to slight rearrangement of the backbone near residues 21–24 and hence slight movement of U20. In the second independent trajectory, both reverse G•U wobble hydrogen bonds are maintained throughout the trajectory (Figure S1F), but the  $\text{Mg}_{\text{rev}}$  moves away and is replaced by a  $\text{Na}^+$  ion (not shown). Thus, the hydrogen bonds within the reverse G•U wobble are maintained when C75 is deprotonated, although the hydrogen-bonding interactions may be slightly weakened.

**B. Metal Ion Interactions with the Reverse and Standard GU Wobbles.** In this subsection, we analyze and compare the interaction of metal ions with the reverse G25•U20 wobble and with the major groove near the standard G1•U37 wobble. These two metal ion interaction sites are separated by a distance of  $\sim 15 \text{ \AA}$  in the C75 precleaved structure. We showed previously that the crystallographically resolved  $\text{Mg}^{2+}$  interacting with the reverse G25•U20 wobble remains bound and is relatively stationary during MD trajectories.<sup>16</sup> In the present work, we observe that  $\text{Mg}^{2+}$  interactions with the standard G1•U37 wobble are qualitatively different. In some trajectories, a  $\text{Mg}^{2+}$  ion near the Hoogsteen face of G35,  $\sim 7 \text{ \AA}$  from the major groove of the standard G•U wobble in the C75 precleaved crystal structure, moves closer to the standard G•U wobble, where it is relatively mobile, while in other instances  $\text{Na}^+$  ions occupy this region. Thus, while  $\text{Mg}_{\text{rev}}$  may be viewed as “chelated” at the reverse G•U wobble, the  $\text{Mg}^{2+}$  interaction in the region

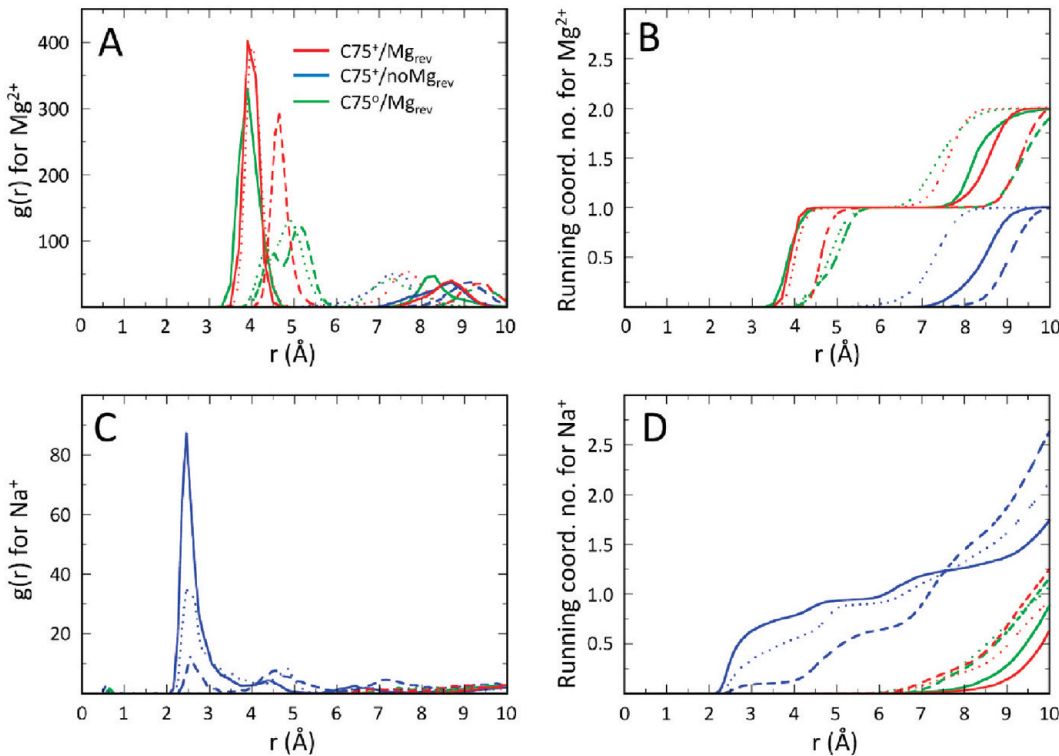


**Figure 4.** Analysis of metal ion interaction at the reverse G25•U20 wobble. Radial distribution functions (panels A and C) and running coordination numbers (panels B and D) are plotted for  $Mg^{2+}$  ions (panels A and B) and  $Na^+$  ions (panels C and D) with respect to G25(N7) (dashed line), G25(O6) (dotted line), and U20(O2) (solid line) atoms of the reverse wobble. Results are provided for  $C75^+/Mg_{rev}$  (red),  $C75^+/noMg_{rev}$  (blue) and  $C75^\circ/Mg_{rev}$  (green) trajectories.

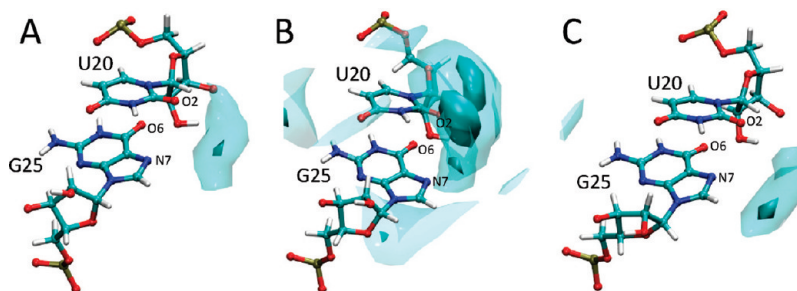


**Figure 5.** Charge isodensity plots in the region of the reverse G25•U20 wobble for (A)  $C75^+/Mg_{rev}$ , (B)  $C75^+/noMg_{rev}$ , and (C)  $C75^\circ/Mg_{rev}$  trajectories. The darker cyan represents the greatest 30% of the positive charge density, and the lighter cyan represents the greatest 80% of the positive charge density. The positive charge density is due predominantly to  $Mg^{2+}$  in panels A and C and to  $Na^+$  in panel B. Stereoview of panel A is provided as Supporting Information, Figure SSD.

near the standard G•U wobble may be viewed as “diffuse”, as defined by Draper.<sup>44</sup>

Radial distribution functions between metal ions and the reverse G•U wobble atoms G25(N7), G25(O6), and U20(O2) for the three types of trajectories help define these interactions and are depicted in Figure 4. These radial distribution functions, as well as the corresponding running coordination numbers, were generated for both  $Mg^{2+}$  and  $Na^+$  ions. Charge isodensity plots representing the spatial distribution of the total amount of positive charge for the three types of trajectories are provided in Figure 5. The combination of these two types of analyses provides insight into the metal ion interactions.

For the  $C75^+/Mg_{rev}$  trajectory, a single  $Mg^{2+}$  was persistently located within  $\sim 4.5$  Å of all three specified atoms of the reverse

G•U wobble, as indicated by the radial distribution plot and the running coordination number with sharp step-like behavior to unity at this distance (Figure 4A,B, red lines). Because  $Mg^{2+}$  remained bound for the entire trajectory, no  $Na^+$  was observed in this region (Figures 4C and D, red lines). The charge isodensity analysis provides further confirmation of this behavior. For the  $C75^+/Mg_{rev}$  trajectory (Figure 5A), the  $Mg^{2+}$  was highly localized near the O6 of G25 and the O2 of U20. The second independent  $C75^+/Mg_{rev}$  trajectory exhibited qualitatively similar behavior (Figures S4 and SSA, and SSD for stereoview).

For the  $C75^+/noMg_{rev}$  trajectory, the  $Mg^{2+}$  was removed from this region prior to equilibration, and no other  $Mg^{2+}$  was observed to move into this region. Instead, a  $Na^+$  ion moved into this vicinity and was located within  $\sim 2.5$  Å of all three specified

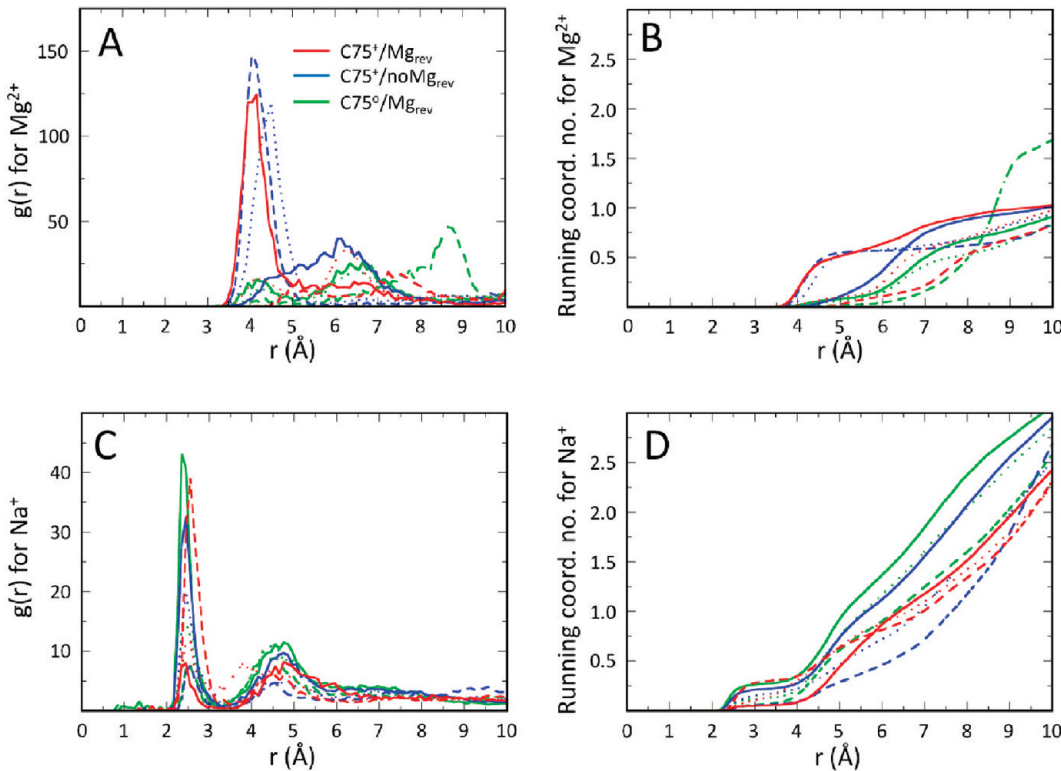


**Figure 6.** Analysis of metal ion interaction at the standard G1•U37 wobble. Radial distribution functions (panels A and C) and running coordination numbers (panels B and D) are plotted for  $Mg^{2+}$  ions (panels A and B) and  $Na^+$  ions (panels C and D) with respect to G1(N7) (dashed line), G1(O6) (dotted line) and U37(O2) (solid line) atoms of the standard wobble. Results are provided for  $C75^+/Mg_{rev}$  (red),  $C75^+/noMg_{rev}$  (blue), and  $C75^\circ/Mg_{rev}$  (green) trajectories.

atoms of the reverse G•U wobble for a significant portion of the trajectory (Figure 4C,D, blue lines). In this case, however, the running coordination number (Figure 4D) does not reach unity until larger distances and does not exhibit sharp step-like behavior as in Figure 4B. This behavior indicates that  $Na^+$  did not remain in this region throughout the entire trajectory. Thus, the  $Na^+$  ion was relatively mobile compared to the  $Mg^{2+}$  in the  $C75^+/Mg_{rev}$  trajectory. This behavior was confirmed by analysis of the charge isodensity plot. For the first  $C75^+/noMg_{rev}$  trajectory (Figure 5B), the positive charge density was relatively delocalized, corresponding to the more mobile  $Na^+$  that replaced the removed  $Mg_{rev}$ . In the second independent  $C75^+/noMg_{rev}$  trajectory (Figure S5B), the  $Na^+$  ion was more localized near the O2 of U20 than in the first trajectory. This observation is consistent with the radial distribution functions for this second trajectory (Figure S4C,D, blue lines), which exhibit a peak at  $\sim 2.5 \text{ \AA}$  for U20(O2) (solid blue line), with a corresponding running coordination number of nearly unity at this distance but no peaks for G25(N7) (dashed blue line) or G25(O6) (dotted blue line). Thus, the  $Na^+$  ion is localized near O2 of U20 for the second trajectory but is delocalized over a much larger region for the first trajectory.

The two  $C75^\circ/Mg_{rev}$  trajectories exhibited different behavior. In particular, the  $Mg^{2+}$  remained bound to the reverse G•U wobble throughout the first trajectory (Figure 4A,B, green lines), but it moved away and was replaced by a  $Na^+$  ion in the second trajectory (Figure S4, green lines). This behavior is also illustrated by the charge isodensity plots. For the first  $C75^\circ/Mg_{rev}$  trajectory (Figure 5C), the  $Mg^{2+}$  was highly localized, with a

distribution similar to that for the  $C75^+/Mg_{rev}$  trajectory. In the second independent  $C75^\circ/Mg_{rev}$  trajectory (Figure SSC), the  $Mg^{2+}$  was replaced by the more mobile  $Na^+$ , leading to a more delocalized positive charge distribution (compare Figures SSC and 5C). As discussed above, deprotonation of C75 leads to structural rearrangements of the active site, including the loss of hydrogen bonding at C75 to the leaving group, displacement of the O2' of U-1 from  $Mg_{rev}$ , and the slight weakening of hydrogen-bonding interactions within the reverse G•U wobble (Figures 3, S1, and S3). The replacement of the  $Mg_{rev}$  by  $Na^+$  in the second trajectory may be linked to these structural rearrangements at the active site. Nevertheless, the reverse G•U wobble still appears to effectively interact with either a divalent or monovalent metal ion, even when C75 is deprotonated.

We also performed the same analyses for the standard G1•U37 wobble (radial distribution functions in Figures 6 and S6 and charge isodensity plots in Figure 7 and S7). In this case, both hydrogen bonds within the standard wobble were maintained for all trajectories, which is consistent with our experiments that supported the importance of a stable base pair at this position.<sup>26</sup> The region containing the standard G•U wobble and P1.1 (G38, G39) just below provides a favorable negative pocket for cationic metal ions (see below). The radial distribution functions and running coordination numbers for the  $C75^+/Mg_{rev}$  and  $C75^+/noMg_{rev}$  trajectories (Figure 6 and S6, red and blue lines, respectively) indicate an intermittent presence of  $Mg^{2+}$  and  $Na^+$  in this region. When present (Figure 6A,B), the  $Mg^{2+}$  moved into the standard G•U wobble region from its crystallographic position near the G35 Hoogsteen face, which is further

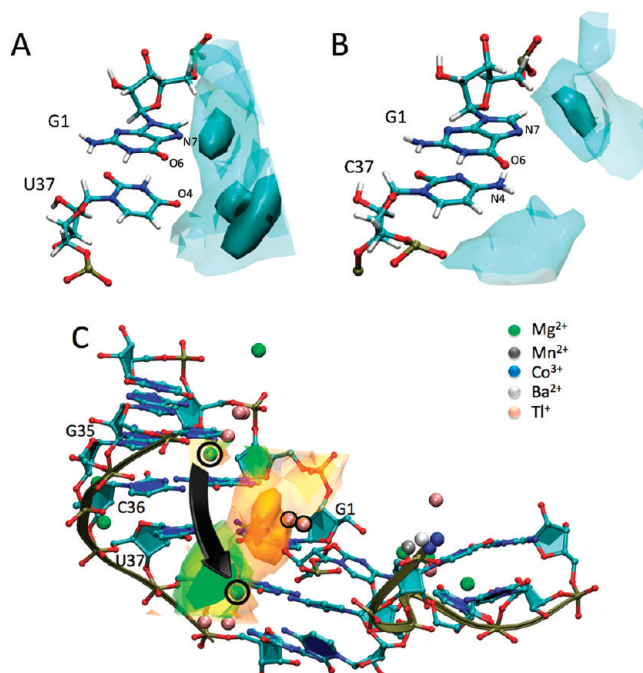


**Figure 7.** Metal ion interactions near the standard G•U wobble. Charge isodensity plots in the region of the (A) G1•U37 standard wobble in the wild-type and (B) G1•C37 Watson–Crick base pair in the U37C mutant for the  $C75^+$ /Mg<sub>rev</sub> trajectories. The darker cyan represents the greatest 30% of the positive charge density, and the lighter cyan represents the greatest 80% of the positive charge density. The positive charge density is due to both Mg<sup>2+</sup> and Na<sup>+</sup>. Stereoview of panel A is provided as Supporting Information, Figure S7D. (C) Comparison of divalent and monovalent ions from theoretical and experimental methods overlap. Charge isodensity plots for Mg<sup>2+</sup> (green) and Na<sup>+</sup> (amber) ions in the region of the G1•U37 normal wobble are shown in the center. This portion of the figure is the same as panel A except that Mg<sup>2+</sup> and Na<sup>+</sup> are depicted separately in green and amber, respectively, and the view is rotated ~90° about the vertical axis to better view the major groove of P1/P1.1. These plots are superimposed with crystallographically resolved metal ions from multiple HDV ribozyme structures, showing location of divalent and monovalent ions, which are colored similarly (see key for all ion identities). The arrow depicts motion of a Mg<sup>2+</sup> ion observed during the early stages of the  $C75^+$ /Mg<sub>rev</sub> trajectory. The Mg<sup>2+</sup> ion at the start of the arrow is present at G35 in crystal structure 3NKB, and the Mg<sup>2+</sup> ion at the end of the arrow is present at P1.1 in crystal structure 1CX0. The monovalent ions are Tl<sup>+</sup> ions present in crystal structure 2OJ3.

up P1. Movement of this ion is shown with an arrow in Figure 7C, where the starting and ending points of the arrow also happen to correspond to crystallographic Mg<sup>2+</sup> ions, albeit from two different structures (3NKB and 1CX0).<sup>8,21</sup> When this movement of the Mg<sup>2+</sup> ion was observed, it typically occurred during the first 5–10 ns of the trajectory. When the Mg<sup>2+</sup> ion was absent, Na<sup>+</sup> monovalent ions were in this region instead, which is characteristic of diffuse sites.<sup>44</sup> For the  $C75^+$ /Mg<sub>rev</sub> trajectories (Figures 6 and S6, green lines), the region near the standard G•U wobble was occupied mainly by Na<sup>+</sup> ions, again characteristic of diffuse sites.

The charge isodensity plots for the standard G1•U37 wobble (Figures 7A and S7) illustrate that the positive charge density was delocalized over the region near the standard G•U wobble for all trajectories (Figure S7D for stereoview), indicating diffuse metal ions. In addition, the charge isodensity plot for Mg<sup>2+</sup> overlaid

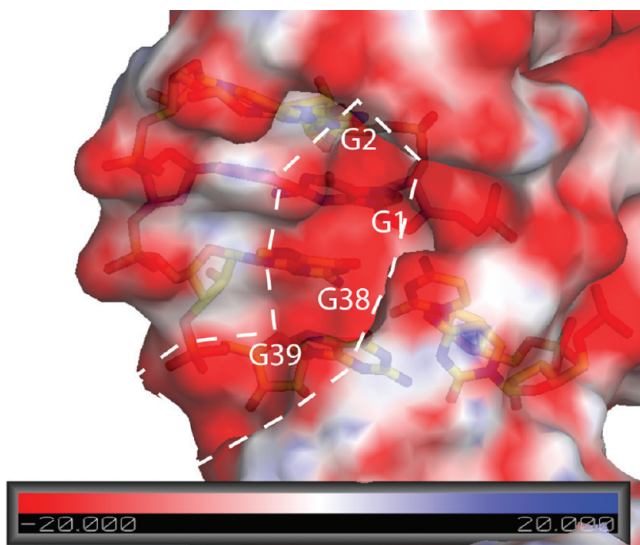


**Figure 8.** Nonlinear Poisson–Boltzmann (NLPB) electrostatic potential for a snapshot obtained after 25 ns of simulation for a  $C75^+$ /Mg<sub>rev</sub> trajectory. Potential is colored according to the gradient scale at bottom of the panel (−20 kT/e to +20 kT/e). Surface is shown with 20% transparency. View is of the major groove of the G1•U37 wobble, the G2•C36 base pair above, and the two P1.1 GC base pairs below involving G38 and G39. A diffuse negative patch involving these four base pairs is observed, outlined with a dashed line.

well with positioning of Mg<sup>2+</sup> from crystallography, and a similar plot for Na<sup>+</sup> overlaid well with position of Tl<sup>+</sup>, a heavy monovalent ion, from crystallography (Figure 7C). This observation suggests that charge isodensity calculations are reflective of experimentally determined favorable ion interactions. In summary, behavior near the reverse and standard G•U wobbles contrasts strongly (compare  $C75^+$ /Mg<sub>rev</sub> trajectories in Figures 5A and 7A), suggestive of chelation in the former and a diffuse ion atmosphere in the latter.

Nonlinear Poisson–Boltzmann (NLPB) calculations in the regions of these two G•U wobbles provide a plausible explanation for these two qualitatively different types of interactions. As shown in Figure 8, the potential near the standard G•U wobble is ~−20 kT/e, which is similar to previously reported values for tandem G•U wobbles and to that of the phosphate backbone.<sup>45</sup> This negatively charged region extends up P1 into the vicinity of the G2 and down P1.1 into the vicinity of G38 and G39. This potential is very different from that at the reverse G•U wobble, where the potential was much more negative (~−150 kT/e) and more localized.<sup>16</sup> These qualitatively different potentials are consistent with a more mobile and diffuse ion atmosphere near the standard G•U wobble and a less mobile and chelating ion near the reverse G•U wobble.

As mentioned above, the standard G•U wobble is sometimes replaced by a standard Watson–Crick GC or AU base pair in nature. We therefore analyzed the effect of a U37C mutation, leading to a GC base pair, on hydrogen-bonding interactions at the active site and on the metal interaction with both the reverse and standard G•U wobbles. For this purpose, we propagated trajectories of the U37C mutant of the type  $C75^+$ /Mg<sub>rev</sub>, where the crystallographic catalytic Mg<sup>2+</sup> was included and the C75 was protonated. As shown in Figure S8, all three of the hydrogen bonds involving C75 remained stable in the mutant; in addition, the standard hydrogen bonding in the GC base pair was retained

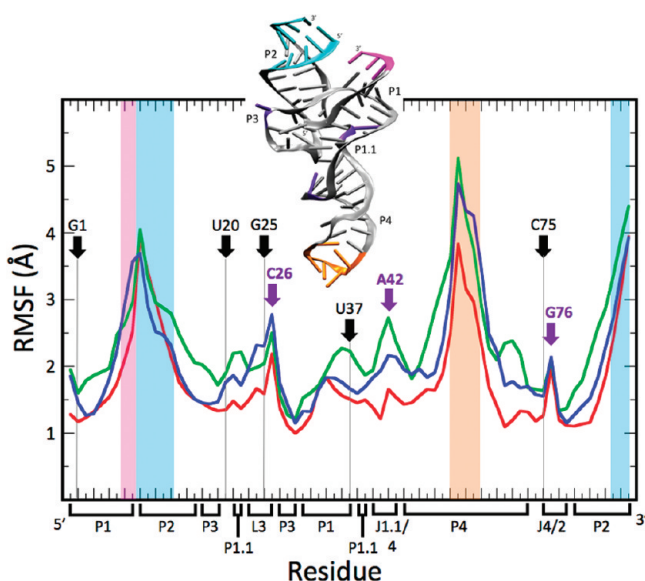


**Figure 9.** Root mean square fluctuations (RMSFs) of heavy atoms for each residue of the HDV ribozyme. Results are provided for  $C75^+/\text{Mg}_{\text{rev}}$  (red line),  $C75^+/\text{noMg}_{\text{rev}}$  (blue line), and  $C75^\circ/\text{Mg}_{\text{rev}}$  (green line) trajectories. Regions of the ribozyme, as shown in Figure 1, are identified on the  $x$ -axis. Residues exposed to the solvent are indicated by violet arrows. Key residues of the active site are indicated by black arrows. Regions of the ribozyme displaying a particularly large RMSF are shown by pink, cyan, and orange regions. Corresponding regions are also marked in the three-dimensional cartoon representation.

(Figure 7B). We also found that the  $\text{Mg}_{\text{rev}}$  remained bound, as in the analogous wild-type trajectories. As shown in Figure 7B, the positive charge density near the G1-C37 region was qualitatively similar to that observed in the wild-type trajectories (Figure 7A), except for a shift in the positive charge density away from the N4 atom of residue 37, as expected for the keto to amine change associated with the mutation of U to C. This shift in the positive charge density was also observed for a second independent trajectory of the U37C mutant (Figure S9), where a lack of charge density is found near the 4 position of C37.

**C. Atomic Fluctuations and Correlated Motions.** We investigated whether changes in C75 protonation and  $\text{Mg}^{2+}$  interactions at the reverse G•U wobble affect the global structure or motion of the ribozyme. The root-mean-square deviations (RMSDs) between the thermally averaged structures for the  $C75^+/\text{Mg}_{\text{rev}}$  and  $C75^\circ/\text{Mg}_{\text{rev}}$  trajectories and for the  $C75^+/\text{Mg}_{\text{rev}}$  and  $C75^+/\text{noMg}_{\text{rev}}$  trajectories are relatively small, as shown in Tables S1 and S2, respectively. These RMSDs thus indicate that the global structure is not significantly affected by C75 protonation or  $\text{Mg}_{\text{rev}}$ . Note that deprotonation of C75 has a slightly larger effect on the RMSD (Table S1) of the active site than does removal of  $\text{Mg}_{\text{rev}}$  (Table S2), consistent with the above analysis.

The root-mean-square fluctuations (RMSFs) of the residues for the  $C75^+/\text{Mg}_{\text{rev}}$ ,  $C75^+/\text{noMg}_{\text{rev}}$ , and  $C75^\circ/\text{Mg}_{\text{rev}}$  trajectories are depicted in Figure 9. The RMSFs are qualitatively similar for all three trajectories, as well as for the second set of independent trajectories (Figure S10). In all cases, the terminal residues at the top of P1 (magenta region), P2 (cyan region), and P4 (orange region) exhibit the greatest fluctuations. The solvent exposed and bulged residues (violet arrows identifying C26, A42, and G76) also exhibited significant fluctuations. The other regions did not fluctuate significantly during these trajectories, other than typical thermal motions of  $1\text{--}2\text{\AA}$ .

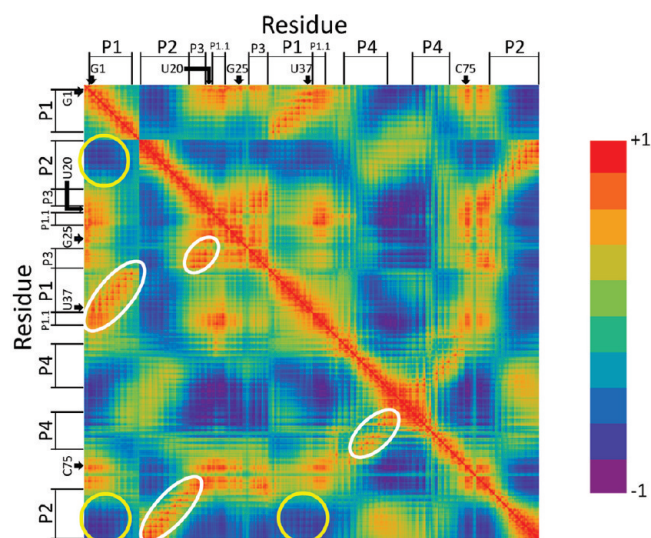


**Figure 10.** Cross-correlation matrix of the heavy atom motions for the  $C75^+/\text{Mg}_{\text{rev}}$  trajectory. Regions of the ribozyme, as shown in Figure 1, are identified on both axes. Certain key residues are highlighted on the axes with black arrows. Red regions indicate correlated motions, and blue regions indicate anticorrelated regions. Helical regions, whose 5' and 3' strands exhibit correlated motions, are identified by white ovals. Certain anticorrelated regions are highlighted by yellow circles.

The cross-correlation matrix for the heavy atoms in the  $C75^+/\text{Mg}_{\text{rev}}$  trajectory is plotted in Figure 10. Cross-correlation matrices for the  $C75^+/\text{noMg}_{\text{rev}}$  and  $C75^\circ/\text{Mg}_{\text{rev}}$  trajectories are qualitatively similar and are provided in Figure S11. Red regions indicate pairs of atoms that are moving in the same direction (i.e., correlated), and blue regions indicate pairs of atoms that are moving in the opposite direction (i.e., anticorrelated). The red diagonal regions perpendicular to the main diagonal represent strands of helical regions that are moving together. Helical regions corresponding to P1, P2, P3, and P4 are evident in Figure 10 (white ellipses). In addition, correlated motions extend along the two aforementioned coaxial helical stacks: P2 and P3, which form one coaxial stack, are correlated, as are P1 and P1.1, and P1.1 and the top of P4, which together form an extended coaxial stack. In terms of anticorrelated motions, the P1 helix moves in the opposite direction from the P2 helix (Figure 10, yellow circles). Anticorrelated motions are also found near L4 (the loop of P4); however, this region is not part of the native structure.<sup>8</sup>

Focusing on the reverse and standard G•U wobbles, we observed strongly anticorrelated motions between G25 and U37 for all three types of trajectories (Figures 11 and S12). This observation suggests that the reverse and standard G•U wobbles are moving in opposite directions, despite the distance of  $\sim 23\text{\AA}$  between residues G25 and U37. This behavior is also observed in the absence of  $\text{Mg}_{\text{rev}}$  and C75 protonation (Figure S12), suggesting that it is not due solely to the positive charge on the metal or C75. The possible connection of these anticorrelated motions to catalysis is a direction for future research.

#### IV. DISCUSSION

In the Discussion, we compare the simulations and calculations to experimental data. Overall, we find broad consistency between theory and experiment. The Discussion is organized

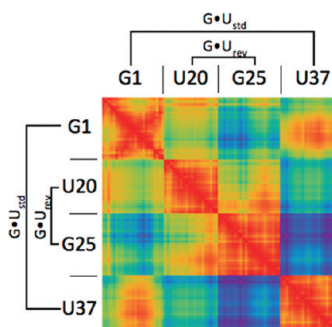


**Figure 11.** Cross-correlation matrix of the heavy atom motions in the reverse ( $\text{G}25\bullet\text{U}20$ ) and standard ( $\text{G}1\bullet\text{U}37$ ) wobbles for the  $\text{C}75^+/\text{Mg}_{\text{rev}}$  trajectory. As in Figure 10, red regions indicate correlated motions, and blue regions indicate anticorrelated motions.

into the same three subsections as the Results. We note that this paper focuses on only the ground reactant state of the ribozyme and does not examine the relative stabilities of the reactant, transition, and product states. An assessment of the impact of metal binding and  $\text{C}75$  protonation on the catalyzed chemical reaction would require an investigation of the reaction pathway and the associated free energy barriers, which is beyond the scope of the present work.

**A. Active Site Hydrogen Bonding Interactions.** The hydrogen-bonding interactions at  $\text{C}75^+$  and the reverse  $\text{G}\bullet\text{U}$  wobble presented in Figures 3 and S1 suggest that the catalytic  $\text{Mg}^{2+}$  ion and  $\text{C}75$  protonation provide structural stability to the active site. For the  $\text{C}75^+/\text{Mg}_{\text{rev}}$  trajectories, observation that the hydrogen bonds involving  $\text{C}75^+$  and within the reverse  $\text{G}\bullet\text{U}$  wobble base pair are well-formed throughout the trajectories suggests that this state of the ribozyme is particularly stable. This observation is consistent with catalytic competence of this state, in which  $\text{C}75^+$  acts as the general acid to protonate the 5'-bridging oxygen of  $\text{G}1$ , and the  $\text{Mg}^{2+}$  ion at the reverse wobble acts as the Lewis acid (Figure 1B).<sup>8</sup> The initial structure of the HDV ribozyme bound to its substrate was generated by superimposing the cleavage site dinucleotide from the hammerhead ribozyme onto the HDV ribozyme active site. In the resulting model it was not adjusted further and, therefore, the  $\text{C}75(\text{N}3)-\text{G}1(\text{O}5')$  bond was long at 3.6 Å. During the MD trajectories,  $\text{C}75(\text{N}3)$  and  $\text{G}1(\text{O}5')$  moved to within hydrogen bonding distance of each other. Thus, the MD supports and refines the model generated from the crystal structure.

For the  $\text{C}75^+/\text{noMg}_{\text{rev}}$  trajectories, the behavior of  $\text{C}75^+$  and the reverse  $\text{G}\bullet\text{U}$  base pair in the absence of  $\text{Mg}_{\text{rev}}$  has implications for the mechanism of channel 1 of the HDV ribozyme, wherein reaction is promoted in the presence of  $\text{Na}^+$  ions without divalent ions. Observation that  $\text{C}75$  is positioned in a catalytically competent fashion at least part of the time without  $\text{Mg}_{\text{rev}}$  is consistent with experiments that support  $\text{C}75$  acting as the general acid under these conditions with a reduced rate.<sup>15</sup> Additionally, these observations are largely consistent with product and precleaved crystal structures being very similar in overall geometries despite absence of the catalytic  $\text{Mg}^{2+}$  ion in the crystal structure of the HDV ribozyme product.<sup>8,12</sup> For the  $\text{C}75^+/\text{Mg}_{\text{rev}}$  trajectories, observation that  $\text{C}75$  does not remain in the crystallographically observed hydrogen-bonding patterns and that the  $\text{O}2'$  of  $\text{U}-1$  is no longer engaged with the catalytic  $\text{Mg}^{2+}$  ion suggests that protonation of  $\text{C}75$  in the precleaved state assists in organizing the active site. This point is also

illustrated by an overlay of the thermally averaged structures from the  $\text{C}75^+/\text{Mg}_{\text{rev}}$  and  $\text{C}75^\circ/\text{Mg}_{\text{rev}}$  trajectories, which revealed loss of catalytic positioning upon deprotonation (Figure S2). The result that deprotonation of  $\text{C}75$  in the precleavage state disrupts the local active site structure is distinct from that of Walter and co-workers, who suggested that the  $\text{C}75$  position changes during the catalytic reaction.<sup>46</sup> Further studies may reveal whether these two observations are related.

These changes in conformation afforded by  $\text{C}75$  protonation are likely local accommodations rather than global, as supported by three observations. First, comparison of the thermally averaged structures in the  $\text{C}75^+$  and  $\text{C}75^\circ$  states reveals only small RMSDs in atom positions, especially in the active site (Table S1). Second, the overall geometry of the product and precleaved crystal structures, which are likely deprotonated and protonated, respectively,<sup>18,47</sup> are similar.<sup>8,12</sup> Third, there is a lack of large changes in Raman signal upon protonation of  $\text{C}75$  in precleaved HDV ribozyme crystals.<sup>18</sup>

The recent crystal structure of the HDV ribozyme reveals a  $\text{Mg}^{2+}$  ion in proximity to the cleavage site. Its position relative to  $\text{C}75$  and the  $\text{G}1(\text{O}5')$  led us to propose that this ion participates in catalysis by acting as a Lewis acid, facilitating the deprotonation of the  $\text{U}-1(\text{O}2')$  nucleophile.<sup>8</sup> In this model of the HDV ribozyme in the precleaved state,  $\text{Mg}^{2+}$  interacts with both  $\text{U}-1(\text{O}2')$  and  $\text{G}1(\text{O}2\text{P})$ . The interaction between  $\text{Mg}^{2+}$  and the scissile phosphate is supported by the deleterious effect of sulfur substitution at  $\text{G}1(\text{O}2\text{P})$ .<sup>48</sup> Proton inventory experiments in the presence and absence of  $\text{Mg}^{2+}$  are consistent with  $\text{Mg}^{2+}$ -facilitated deprotonation of the  $\text{U}-1(\text{O}2')$ ,<sup>15,49</sup> although direct interaction between  $\text{U}-1(\text{O}2')$  and the active site  $\text{Mg}^{2+}$  ion has never been directly probed. The MD trajectories described here explore the feasibility of this model by examining the stability of the interactions between  $\text{Mg}_{\text{rev}}$  and both  $\text{U}-1(\text{O}2')$  and  $\text{G}1(\text{O}2\text{P})$ . The stable interaction maintained throughout both  $\text{C}75^+/\text{Mg}_{\text{rev}}$  trajectories (Figure S3) is consistent with the proposed model corresponding to a reactive conformation.

**B. Metal Ion Interactions with the Reverse and Standard  $\text{G}\bullet\text{U}$  Wobbles.** Analysis of metal ion interaction at the reverse and standard  $\text{G}\bullet\text{U}$  wobbles is consistent with a chelated ion at the reverse  $\text{G}\bullet\text{U}$  wobble and a diffuse monovalent or divalent ion interaction at the standard  $\text{G}\bullet\text{U}$  wobble. Presence of both monovalent and divalent ions in the vicinity of the standard  $\text{G}\bullet\text{U}$  wobble is diagnostic of diffuse sites.<sup>44</sup> For the reverse  $\text{G}\bullet\text{U}$  wobble, the electrostatic potential was exceptionally negative at  $\sim -150 \text{ kT/e}$ <sup>16</sup> as expected for chelated sites,<sup>45</sup> the radial distribution functions exhibited sharp peaks with running coordination numbers of unity at binding distances (Figure 4), and the charge isodensity plots indicated highly localized interaction (Figure 5). In contrast, for the standard  $\text{G}\bullet\text{U}$  wobble, the electrostatic potential was only  $\sim -20 \text{ kT/e}$  (Figure 8) as expected for this type of motif,<sup>45</sup> the radial distribution functions were less sharp with fractional running coordination numbers at binding distances (Figure 6), and the charge isodensity plots indicated diffuse ion interaction (Figure 7). These differences in metal ion interactions at the two types of  $\text{G}\bullet\text{U}$  wobbles arise from the greater magnitude and higher localization of the negative charge in the pocket at the reverse  $\text{G}\bullet\text{U}$  wobble, as compared to the weaker and more delocalized negative charge near the standard  $\text{G}\bullet\text{U}$  wobble, which extends up P1 and down into P1.1 (Figure 8).

A diffuse ion atmosphere near the standard  $\text{G}\bullet\text{U}$  wobble is also supported by prior experiments from our laboratories that used

7-deazaguanosine (i.e., N7 changed to a C–H) single and double substitutions at G1 and G2 in the HDV ribozyme substrate.<sup>50</sup> These variant RNAs, which have lessened negative potential in the major groove, reacted more than 10 times slower than wild-type in the double mutant. Raman spectroscopic characterization of a ribozyme crystal with a single 7-deazaguanosine substitution at G1 revealed a loss of interaction between N7 and a Mg<sup>2+</sup> ion; however, the Mg<sup>2+</sup> dependence of the ribozyme reaction was only subtly perturbed. The observation that the 7-deazaguanosine-modified RNAs still bound Mg<sup>2+</sup> avidly in spite of the loss of interaction with G1(N7) is again consistent with a diffuse site. Loss of a factor of 10 in rate with the double deazaguanosine mutant suggests that the metal ion at the standard G•U position could contribute to rate enhancement, possibly by affecting folding (see below).

Our MD simulations indicated qualitatively similar behavior for the U37C mutant and the wild-type HDV ribozyme in terms of the active site hydrogen-bonding interactions, as well as the metal ion interactions with the reverse and standard G•U wobbles. This observation is consistent with the known occurrence of GC and AU Watson–Crick base pairs in HDV and HDV-like ribozymes at this position.<sup>9,10,25</sup> It is also consistent with the experimental determination that AU or GC at the cleavage site gives indistinguishable reaction kinetics and Mg<sup>2+</sup> dependence.<sup>26</sup>

Draper has argued that diffuse metal ions are major factors in stabilizing RNA tertiary structures.<sup>44</sup> Thus, one possibility is that the ion at the junction of P1 and P1.1 plays a role in stabilizing the tertiary fold of the RNA, where it imparts stability from entropy gain in delocalizing along the RNA.<sup>44,51</sup> In contrast, the ion at the reverse G•U wobble plays a role in catalyzing the reaction as a Lewis acid, where fixing its position is likely critical for chemistry to occur. The two-base pair P1.1 helix is one of the smallest helices observed in any functional RNA, and it is often just one base pair in the HDV-like ribozymes;<sup>10</sup> thus, it seems that this region could benefit from added tertiary structure stabilization. The HDV ribozyme is known to be exceptionally stable, with a melting temperature for tertiary structure of ~75 °C in just 0.1 mM Mg<sup>2+</sup>.<sup>11</sup> Such exceptional stability is consistent with the relative independence of C75 protonation and metal ion interaction to the reverse and standard G•U wobbles.

**C. Atomic Fluctuations and Correlated Motions.** Essentially no differences in the RMSF and cross-correlation plots were found among the various C75 protonation and Mg<sup>2+</sup>-bound states of the ribozyme. The RMSF analysis indicates that the larger thermal motions are limited to the periphery of the ribozyme, while the core of the ribozyme exhibits only relatively small thermal motions. Correlated motions were found within each helix, as well as between the coaxial stacks of P2/P3 and P1/P1.1/P4. These observations suggest that the ribozyme exists as at least two somewhat stiff rods. Interestingly, portions of these two stacks appear to be anticorrelated with each other. In particular, P1 and P2 are strongly anticorrelated. Moreover, the motions of G25 and U37 also appear to be anticorrelated. Whether these motions contribute to catalysis, perhaps by aligning reactive functionalities, is unclear at present.

This analysis suggests that the chemical reaction pathway of the HDV ribozyme is dominated by small local motions at the active site and does not rely on large-scale global conformational changes. The roles of short-range and long-range motions in protein enzymes have been investigated extensively.<sup>52,53</sup> In most protein enzymes, small local motions in the active site are

required to facilitate catalysis, and in some cases, relatively large loop motions are essential to accommodate ligand binding and product release. In many enzymes, equilibrium thermal motions throughout the enzyme assist in the preorganization of the active site and the conformational sampling of configurations conducive to catalysis. The further investigation of short- and long-range motions in ribozymes is a direction for future research.

## V. CONCLUSIONS

We carried out MD simulations to analyze metal ion interaction with a standard and a reverse G•U wobble and to investigate the impact of C75 protonation on the structure and motions of the HDV ribozyme. Importantly, the calculations and simulations herein agree with a wealth of experimental data. We identified two classes of Mg<sup>2+</sup> ions associated with the ribozyme, chelated and diffuse, which appear to contribute to catalysis and stability, respectively. We observed that protonation of C75 locally organizes the active site in a manner that facilitates the catalytic mechanism in which C75<sup>+</sup> acts as a general acid and Mg<sup>2+</sup> as a Lewis acid. On the other hand, protonation of C75 does not alter the global structure and equilibrium thermal motions of the ribozyme. We also found that the catalytic Mg<sup>2+</sup> ion does not significantly impact C75 hydrogen-bonding interactions or the global structure and thermal motions of the ribozyme. Furthermore, our simulations indicate that C75 protonation and the chelated interaction of Mg<sup>2+</sup> to the reverse G•U wobble have virtually no impact on the diffuse metal ion interactions with the standard G•U wobble. In previous studies, we determined that the active site structure, including the reverse G•U wobble with the bound catalytic Mg<sup>2+</sup>, is structurally similar in the precleaved and postcleaved forms,<sup>8</sup> and that protonation has a minimal effect on Raman spectra.<sup>18</sup> These findings, along with the present analysis, suggests that the chemical reaction pathway of the ribozyme is dominated by small local motions at the active site, rather than large-scale global conformational changes.

## ■ ASSOCIATED CONTENT

**S Supporting Information.** Details of equilibration procedure; tables of RMSDs; additional figures depicting data from MD trajectories. This material is available free of charge via the Internet at <http://pubs.acs.org>.

## ■ AUTHOR INFORMATION

### Corresponding Author

\*E-mail: pcb@chem.psu.edu; shs@chem.psu.edu.

## ■ ACKNOWLEDGMENT

We thank Alexander Soudackov and Phil Hanoian for helpful discussions. This project was supported by NIH Grant R01GM095923 (B.L.G. and P.C.B.), NIH Grant GM56207 (S.H.S.), and instrumentation funded by the NSF through Grant OCI-0821527.

## ■ REFERENCES

- (1) DeRose, V. J. *Curr. Opin. Struct. Biol.* 2003, 13, 317–324.
- (2) Hougland, J. L.; Kravchuk, A. V.; Herschlag, D.; Piccirilli, J. A. *PLoS Biol.* 2005, 3, 1536–1548.

- (3) Ferre-D'Amare, A. R.; Scott, W. G. *Cold Spring Harb. Perspect. Biol.* **2010**, a003574.
- (4) Bevilacqua, P. C.; Yajima, R. *Curr. Opin. Chem. Biol.* **2006**, *10*, 455–464.
- (5) Bevilacqua, P. C. Proton Transfer in Ribozyme Catalysis. In *Ribozymes and RNA Catalysis*; Lilley, D. M., Eckstein, F., Eds.; Royal Society of Chemistry: Cambridge, 2008; pp 11–36.
- (6) Nakano, S.; Proctor, D. J.; Bevilacqua, P. C. *Biochemistry* **2001**, *40*, 12022–12038.
- (7) Perrotta, A. T.; Been, M. D. *Biochemistry* **2006**, *45*, 11357–11365.
- (8) Chen, J. H.; Yajima, R.; Chadalavada, D. M.; Chase, E.; Bevilacqua, P. C.; Golden, B. L. *Biochemistry* **2010**, *49*, 6508–6518.
- (9) Salehi-Ashtiani, K.; Luptak, A.; Litovchick, A.; Szostak, J. W. *Science* **2006**, *313*, 1788–1792.
- (10) Webb, C.-H. T.; Riccitelli, N. J.; Ruminski, D. J.; Lupták, A. *Science* **2009**, *326*, 953.
- (11) Nakano, S.; Cerrone, A. L.; Bevilacqua, P. C. *Biochemistry* **2003**, *42*, 2982–2994.
- (12) Ferre-D'Amare, A. R.; Zhou, K.; Doudna, J. A. *Nature* **1998**, *395*, 567–574.
- (13) Nakano, S.; Chadalavada, D. M.; Bevilacqua, P. C. *Science* **2000**, *287*, 1493–1497.
- (14) Das, S. R.; Piccirilli, J. A. *Nat. Chem. Biol.* **2005**, *1*, 45–52.
- (15) Cerrone-Szakal, A. L.; Siegfried, N. A.; Bevilacqua, P. C. *J. Am. Chem. Soc.* **2008**, *130*, 14504–14520.
- (16) Veeraraghavan, N.; Ganguly, A.; Chen, J. H.; Bevilacqua, P. C.; Hammes-Schiffer, S.; Golden, B. L. *Biochemistry* **2011**, *50*, 2672–2682.
- (17) Nakano, S.; Bevilacqua, P. C. *Biochemistry* **2007**, *46*, 3001–3012.
- (18) Gong, B.; Chen, J. H.; Chase, E.; Chadalavada, D. M.; Yajima, R.; Golden, B. L.; Bevilacqua, P. C.; Carey, P. R. *J. Am. Chem. Soc.* **2007**, *129*, 13335–13342.
- (19) Ferre-D'Amare, A. R.; Doudna, J. A. *J. Mol. Biol.* **2000**, *295*, 541–556.
- (20) Ke, A.; Zhou, K.; Ding, F.; Cate, J. H.; Doudna, J. A. *Nature* **2004**, *429*, 201–205.
- (21) Ke, A.; Ding, F.; Batchelor, J. D.; Doudna, J. A. *Structure* **2007**, *15*, 281–287.
- (22) Saenger, W. *Principles of Nucleic Acid Structure*; Springer-Verlag: New York, 1984.
- (23) Siegfried, N. A.; Metzger, S. L.; Bevilacqua, P. C. *Biochemistry* **2007**, *46*, 172–181.
- (24) Sokoloski, J. E.; Godfrey, S. A.; Dombrowski, S. E.; Bevilacqua, P. C. 2011, submitted for publication.
- (25) Chadalavada, D. M.; Cerrone-Szakal, A. L.; Bevilacqua, P. C. *RNA* **2007**, *13*, 2189–2201.
- (26) Cerrone-Szakal, A. L.; Chadalavada, D. M.; Golden, B. L.; Bevilacqua, P. C. *RNA* **2008**, *14*, 1746–1760.
- (27) Tanner, N. K.; Schaff, S.; Thill, G.; Petit-Koskas, E.; Crain-Denoyelle, A. M.; Westhof, E. *Curr. Biol.* **1994**, *4*, 488–498.
- (28) Veeraraghavan, N.; Bevilacqua, P. C.; Hammes-Schiffer, S. *J. Mol. Biol.* **2010**, *402*, 278–291.
- (29) Jorgensen, W. L.; Chandrasekhar, J.; Madura, J. D.; Impey, R. W.; Klein, M. L. *J. Chem. Phys.* **1983**, *79*, 926–935.
- (30) Maestro; version 9.0; Schrödinger L.L.C.: New York, 2010.
- (31) Bowers, K. J.; Chow, E. Xu, H. Dror, R. O. Eastwood, M. P. Gregersen, B. A. Klepeis, J. L. Kolossvary, I. K. Moraes, M. A. Sacerdoti, F. D. Salmon, J. K. Shan, Y. Shaw, D. E. Proceedings of the ACM/IEEE Conference on Supercomputing (SC06), 2006.
- (32) Desmond Molecular Dynamics System; D. E. Shaw Research: New York, 2008.
- (33) Cornell, W. D.; Cieplak, P.; Bayly, C. I.; Gould, I. R.; Merz, K. M. J.; Ferguson, D. M.; Spellmeyer, D. C.; Fox, T.; Caldwell, J. W.; Kollman, P. A. *J. Am. Chem. Soc.* **1995**, *117*, 5179–5197.
- (34) Wang, J. M.; Cieplak, P.; Kollman, P. A. *J. Comput. Chem.* **2000**, *21*, 1049–1074.
- (35) Darden, T.; York, D.; Pedersen, L. *J. Chem. Phys.* **1993**, *98*, 10089–10092.
- (36) Ryckaert, J. P.; Ciccotti, G.; Berendsen, H. J. C. *J. Comput. Phys.* **1977**, *23*, 327–341.
- (37) Nosé, S. *Mol. Phys.* **1984**, *52*, 255–268.
- (38) Hoover, W. G. *Phys. Rev. A* **1985**, *31*, 1695–1697.
- (39) Gilson, M. K.; Sharp, K. A.; Honig, B. *J. Comput. Chem.* **1987**, *9*, 327–335.
- (40) Gilson, M. K.; Honig, B. *Proteins* **1988**, *4*, 7–18.
- (41) Humphrey, W.; Dalke, A.; Schulter, K. *J. Mol. Graphics* **1996**, *14*, 33–38.
- (42) DeLano, W. L. *The PyMOL Molecular Graphics System*; DeLano Scientific: San Carlos, CA, 2002.
- (43) Lindahl, E.; Hess, B.; van der Spoel, D. *J. Mol. Model.* **2001**, *7*, 306–317.
- (44) Draper, D. E. *RNA* **2004**, *10*, 335–343.
- (45) Chin, K.; Sharp, K. A.; Honig, B.; Pyle, A. M. *Nat. Struct. Biol.* **1999**, *6*, 1055–1061.
- (46) Harris, D. A.; Rueda, D.; Walter, N. G. *Biochemistry* **2002**, *41*, 12051–12061.
- (47) Luptak, A.; Ferre-D'Amare, A. R.; Zhou, K.; Zilm, K. W.; Doudna, J. A. *J. Am. Chem. Soc.* **2001**, *123*, 8447–8452.
- (48) Fauzi, H.; Kawakami, J.; Nishikawa, F.; Nishikawa, S. *Nucleic Acids Res.* **1997**, *25*, 3124–3130.
- (49) Nakano, S.; Bevilacqua, P. C. *J. Am. Chem. Soc.* **2001**, *123*, 11333–11334.
- (50) Chen, J. H.; Gong, B.; Bevilacqua, P. C.; Carey, P. R.; Golden, B. L. *Biochemistry* **2009**, *48*, 1498–1507.
- (51) Amzel, L. M. *Proteins* **1997**, *28*, 144–149.
- (52) Benkovic, S. J.; Hammes-Schiffer, S. *Science* **2003**, *301*, 1196–1202.
- (53) Nashine, V. C.; Hammes-Schiffer, S.; Benkovic, S. J. *Curr. Opin. Chem. Biol.* **2010**, *14*, 644–651.